Journal of South American Earth Sciences 48 (2013) 85–96

Contents lists available at ScienceDirect

Journal of South American Earth Sciences

journal homepage: www.elsevier.com/locate/jsames

^{10}Be dating of river terraces of Santo Domingo river, on Southeastern flank of the Mérida Andes, Venezuela: Tectonic and climatic implications

Oswaldo Guzmán [a, b, *], Riccardo Vassallo [b], Franck Audemard [c, d], Jean-Louis Mugnier [b], Javier Oropeza [c], Santiago Yepez [a, e], Julien Carcaillet [f], Miguel Alvarado [g], Eduardo Carrillo [h]

[a] Departamento de Ciencias de la Tierra, Universidad Simon Bolivar, 89000, Caracas 1081-A, Venezuela
[b] ISTerre, Université de Savoie, CNRS, F-73376 Le Bourget du Lac, France
[c] Departamento de Ciencias de la Tierra – Fundacion Venezolana de Investigaciones Sismologicas, Caracas, Venezuela
[d] Escuela de Geología, Minas y Geofísica, Facultad de Ingeniería, Universidad Central de Venezuela, Caracas, Venezuela
[e] Fundacion Instituto de Ingenieria – CPDI, Sartenejas, Venezuela
[f] ISTerre, Université de Grenoble 1, CNRS, F-38041 Grenoble, France
[g] Universidad de Los Andes, Mérida, Venezuela
[h] Instituto de Ciencias de La Tierra, Universidad Central de Venezuela, Venezuela

ARTICLE INFO

Article history:
Received 1 May 2013
Accepted 3 September 2013

Keywords:
Venezuela
Mérida Andes
River terraces
Climatic control
Uplift rate
In situ produced ^{10}Be

ABSTRACT

In this study, we discuss the first cosmogenic ^{10}Be dating of river terraces located in the lower reaches of the Santo Domingo river (Southeastern flank of the Mérida Andes, Western Venezuela). The geomorphic observations and dating allowed the restoration of the temporal evolution of incision rate, which was analysed in terms of tectonic, climatic and geomorphic processes. The long-term incision rate in the area has been constantly around 1.1 mm/a over the last 70 ka. Taking into account the geologic and geomorphologic setting, this value can be converted into the Late Pleistocene uplift rate of the Southeastern flank of the Mérida Andes. Our results show that the process of terraces formation in the lower reaches of the Santo Domingo river occurred at a higher frequency (10^3–10^4 years) than a glacial/interglacial cycle (10^4–10^5 years). According to the global and local climate curve, these terraces were abandoned during warm to cold transitions.

1. Introduction

River terraces are paleotopographic markers, the genesis of which results from tectonics, climatic changes, eustatic variations and geomorphic processes at the catchment scale (Pazzaglia, 2013). The geometrical and sedimentological analysis of river terraces coupled with numerical ages have been widely used in order to decipher and quantify the role of each process (e.g. Maddy et al., 2001; Antoine et al., 2007; Wegmann and Pazzaglia, 2009; Lewin and Gibbard, 2010). The Mérida Andes (MA) is an active tectonic range, located in Western Venezuela (Fig. 1), where several rivers (e.g. Chama, Santo Domingo, Motatán, Guanare, Mocotíes, Tucaní) provide a wide record of river terraces. The origin of these terraces has been mainly associated with Pleistocene paleoclimatic fluctuations (e.g. Zinck, 1980; Vivas, 1984; Schubert and Vivas, 1993), in particular with glacial/interglacial cycles (Tricart and Millies-Lacroix, 1962; Tricart and Michel, 1965; Tricart, 1966). For the terraces located along the axial part of the chain, a tectonic origin associated with the uplift of the chain has also been proposed (Shagam, 1972; Giegengack, 1984; Audemard, 2003). Nonetheless the lack of numerical ages in the river terraces of the MA constitutes a weakness in the argumentation for these two hypotheses.

This study focuses on the Southeastern flank of the MA. The study area is located in the lower reach of Santo Domingo river between the Barinitas city and El Charal village (Fig. 1). In this region, the river presents a series of well-preserved strath terraces, thus the incision rate can be estimated at different time scales. In this reach, the river is orthogonal to the structural trend of the chain; therefore the effect of localized active deformation in the

* Corresponding author. Departamento de Ciencias de la Tierra, Universidad Simon Bolivar, 89000, Caracas 1081-A, Venezuela.
E-mail addresses: oswaldojoseguzman@gmail.com, guzmano@usb.ve (O. Guzmán).

0895-9811/$ – see front matter © 2013 Elsevier Ltd. All rights reserved.
http://dx.doi.org/10.1016/j.jsames.2013.09.004

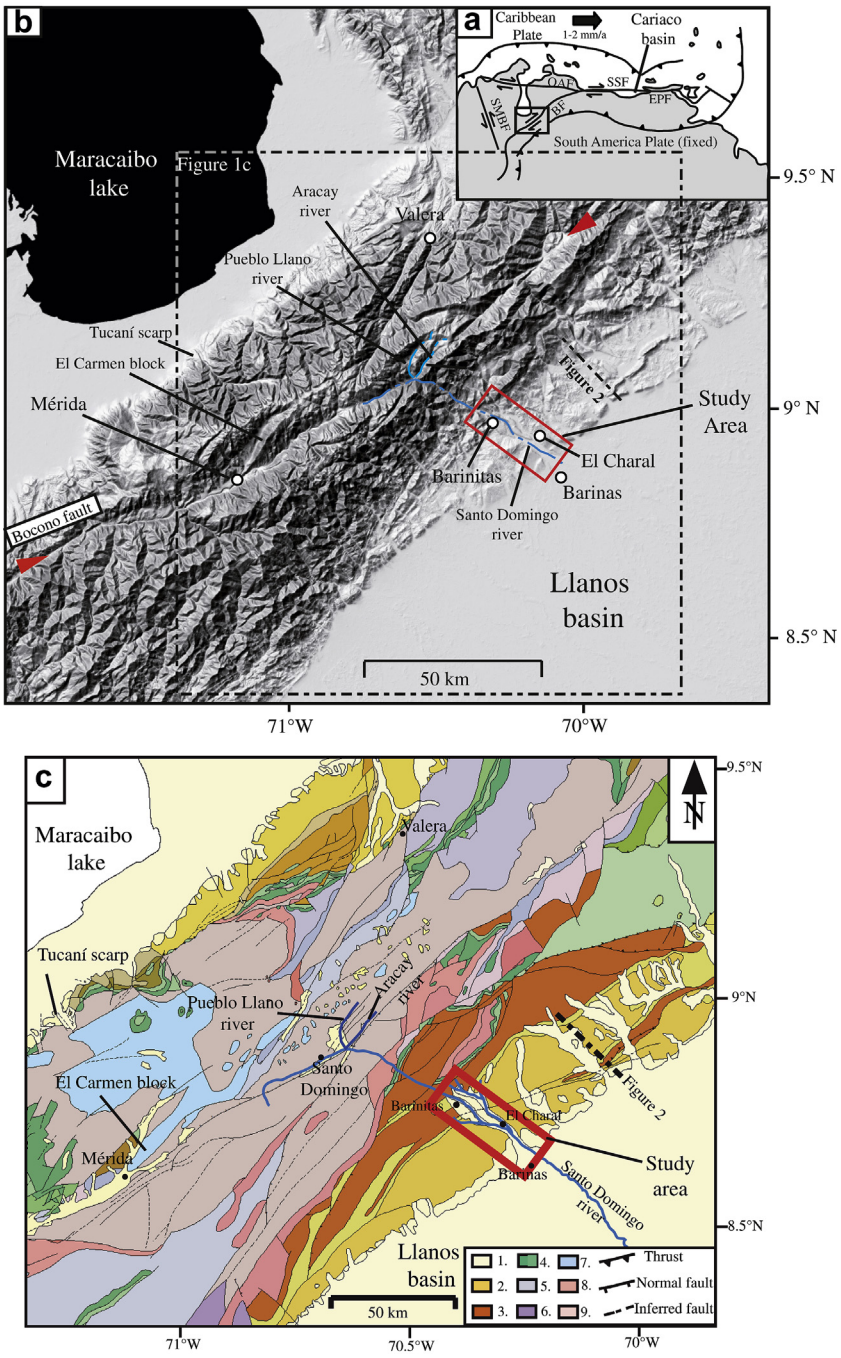

Fig. 1. Geodynamic and morphological settings of the study area. **a**) simplified main present-day active tectonics of Northern South America (from Audemard and Audemard, 2002). (SMBF) Santa Marta Bucaramanga Fault; (OAF) Oca-Ancón Fault; SSF) San Sebastián Fault; (EPF) EL Pilar Fault; (BF) Boconó Fault. Location of the Cariaco basin is shown. **b**) Shaded relief map of the MA based on SRTM. Location of the study area is shown by a red square. Main active trace of the Boconó Fault is located between the two red arrows. **c**) Geological map of the study area from Hackley et al. (2005). 1. Pleistocene to Holocene alluvial sediments; 2. Oligocene, Miocene and Pliocene conglomerates and sandstones; 3. Paleocene to Eocene shales and sandstones; 4. Jurassic to Cretaceous (Undifferentiated) limestones and sandstones; 5. Carboniferous to Permian phylites and limestones; 6. Ordovician to Silurian shales and silstones; 7. Upper Paleozoic to Mesozoic intrusives rocks; 8. Upper to Lower Paleozoic intrusives rocks, phyllites, schist and gneiss; 9. Proterozoic gneiss, schist and granites. Location of Tucaní scarp (Wesnousky et al., 2012) and El Carmen block (Kohn et al., 1984) are also shown. (For interpretation of the references to colour in this figure legend, the reader is referred to the web version of this article.)

process of terraces formation can be quantified. Additionally, the river is far from the sea (more than 1500 km), then the effect of eustatic variation can be neglected. Hence, in this study a morphotectonic analysis is coupled with *in situ* produced ^{10}Be dating (^{10}Be dating, in the text), in order to reconstruct the temporal evolution of the incision rate, which will be analysed in terms of impact of the different processes.

2. Geological setting

The MA is situated in the Western part of Venezuela. This range is around 400 km long with an SW-NE direction from the Colombian-Venezuelan border in the Southwest to Barquisimeto city in the Northeast. The mean elevation of the MA is about 2024 m a.s.l. and culminates at 4978 m a.s.l. at Pico Bolivar, located in the

central part of the chain. The range is bounded on both flanks by the lowlands of the Maracaibo and Llanos basins at the Northwest and Southeast, respectively. Two prominent forebergs are clearly distinguishable along both flanks even if the Southeastern one is better developed (Fig. 1).

The mountain building of MA is related to a complex geodynamic interaction between the Caribbean, South America and Nazca plates and other minor continental blocks (Taboada et al., 2000; Audemard and Audemard, 2002; Bermudez, 2009; Monod et al., 2010). This interaction of plates leads to the oblique convergence between the Maracaibo Triangular Block and South America Plate, and is responsible for the present MA build-up (Colletta et al., 1997; Audemard and Audemard, 2002). This geodynamic setting produces: 1) strain partitioning along the chain, with the NW – SE shortening component accommodated mostly along the two fronts, whereas the dextral component is accommodated along the axis of the range by the Boconó fault (Audemard and Audemard, 2002; Pérez et al., 2011); and 2) tectonic escape process in the central part of the MA (Dhont et al., 2005; Backé et al., 2006).

Current seismicity along the MA occurs within a broad zone, involving the main lineation of the Boconó fault and the entire width of the MA (Audemard and Audemard, 2002). Focal mechanism solutions show mainly a right-lateral faulting along the Boconó fault, left lateral faulting along the North–South trending faults to the North of the MA, and compression along the foothills thrust structures (Audemard, 2003; Colmenares and Zoback, 2003; Corredor, 2003; Cortés and Angelier, 2005). The compression component is distributed through time on different sub-parallel foothills thrusts (e.g. Soulas, 1985; De Toni and Kellogg, 1993; Colletta et al., 1997; Duerto et al., 1998; Audemard, 1999).

Audemard (2003) used the depths of formation of the igneous and metamorphic rocks (8–10 km), located in the highest summits of the chain (~5000 m a.s.l.), to propose a total uplift in the order of 12–15 km for the last 3–5 Ma, and to estimate a rough uplift rate of 2–5 mm/a. Cooling ages derived from apatite fission track analysis of samples from different part of the chain suggest that the long term uplift is diachronic across the MA from Southeast to Northwest (Kohn et al., 1984; Shagam et al., 1984; Bermudez, 2009; Bermudez et al., 2011). It is controlled by the reactivation of pre-existing faults and structures, and the inversion of Jurassic grabens (Kellogg and Bonini, 1982; Colletta et al., 1997; Audemard and Audemard, 2002; Bermudez, 2009). Recently, ^{10}Be dating of boulders on a faulted alluvial fan along the Northwestern foothills (Tucaní scarp – Fig. 1) yielded a Late Pleistocene uplift rate for the Northwestern Andes of ~1.7 ± 0.7 mm/a (Wesnousky et al., 2012).

The MA uplift corresponds to a positive vertical movement of the MA with respect to the Maracaibo and Llanos basins, which are the base levels of the NW and SE running drainage systems, respectively (Fig. 1). This leads to vertical incision by rivers draining the range and consequent formation of fluvial terraces along the rivers located within the chain. These rivers are predominantly oriented in two directions with respect to the axis of the chain: i) Sub-parallel, mainly in the core of the range, and ii) Sub-orthogonal, towards the NW and SE fronts. The Santo Domingo river, located in the central part of MA is flowing along the Southeastern flank from the axis of the chain to the Llanos basin (Fig. 1); in the lower reaches, the Santo Domingo river is orthogonal to the geological structures, thus allowing the study of the late Quaternary incision through them.

3. Paleoclimatic setting

In the MA paleoclimatic information for times prior to the Last Glacial Maximum (~18 ka) comes from glacial and fluvial sequences that have been dated and interpreted in terms of climatic variations (e.g. Schubert and Valastro, 1980; Salgado Labouriau, 1984; Mahaney et al., 2000; Dirszowsky et al., 2005; Rull, 2005). Schubert (1974), based on the presence of two moraine complexes located at different elevations, differentiates an Early and a Late Stage of Mérida glaciation. The age for the Early Stage is poorly constrained. Indeed, only few chronological data are available and they set a lower limiting age at 60 ka (Mahaney et al., 2001; Dirszowsky et al., 2005). The age of the Late Mérida Stage is better constrained. This stage approximately coincides with the global Last Glacial Maximum between 24 and 18 ka (Schubert, 1974; Schubert and Valastro, 1980; Schubert and Clapperton, 1990; Mahaney and Kalm, 1996; Rull, 2005). Lacustrine sediments with buried peat layers between sediments of Early and Late Mérida Stage at the El Pedregal section in central MA suggest interstadial condition (called El Pedregal Interstade). This period is relatively warm and humid, although affected by fluctuating climatic conditions (Mahaney et al., 2001; Dirszowsky et al., 2005; Rull, 2005).

At the scale of Venezuela, the longest paleoclimate record has been obtained in the sediments of Cariaco basin, located in Eastern Venezuela at around 1000 km from the MA (Fig. 1a). Palynological and geochemical analysis of the marine and terrestrial record of this basin (Hughen et al., 1996, 2000; Peterson et al., 2000a, 2000b; González et al., 2008) clearly document the abrupt stadial-interstadial shifts that characterize the Dansgaard/Oeschger cycles (D/O) (Dansgaard et al., 1993) and the Heinrich Events (HE) (Heinrich, 1988) described in North Atlantic marine cores and Greenland ice records over the last ~90 ka. In Cariaco basin, the interstadial warm events are characterized by enhanced marine productivity, increased precipitation and increased river discharge. Stadials cool events show the opposite trends (Peterson et al., 2000a, 2000b; Haug et al., 2001; Peterson and Haug, 2006; González et al., 2008). Heinrich events are characterized by few sediments and lower terrigenous input, with cold and dry conditions almost indistinguishable from stadials (Haug et al., 2001; Peterson and Haug, 2006). The Last Glacial Maximun (LGM – Clark et al., 2009) and the Younger Dryas (YD – Muscheler et al., 2008) have been also documented in the Cariaco basin as cooling and dry periods, occurring between 23 and 21 ka and 13 and 11.8 ka, repectively (Haug et al., 2001; Lea et al., 2003; Hughen et al., 2004). Based on these results, paleoclimatologists concluded that the climate evolution of the Cariaco basin is closely synchronous with the climatic events in the Northern hemisphere even with the rapid climate changes as D/O cycles and Heinrich events.

4. Methods

Field observations, topographic maps at 1:25000 scale (Dirección de Cartografia Nacional, 1976), satellite imagery (Google Earth, 2005) and a 30–m digital elevation model based on the Shuttle Radar Topographic Mission (SRTM) were used to identify and characterize river terraces in the lower reaches of the Santo Domingo river. Alluvial deposit thicknesses and heights of the terraces above the current riverbed were measured using a measuring tape and a laser distancemeter (vertical accuracy ± 0.5 m). Terrace logitudinal profiles were constructed from the digital elevation model and GPS navigator (Etrex®).

The ages of the terraces have been determined by ^{10}Be dating in siliceous rich sand, cobbles or boulders (Lal, 1991; Brown et al., 1991). Six samples were collected from a depth-profile in terrace T2. This sampling strategy allowed the estimation of the ^{10}Be inherited from prior exposure (Anderson et al., 1996; Repka et al., 1997). ^{10}Be inherited component was also estimated from the concentration of ^{10}Be in sediment of active stream bed (Repka et al., 1997; Hancock et al., 1999; Hetzel et al., 2002). This last approach assumes that the inherited concentration is similar to the current

riverbed concentration. For the terraces T3 and T2, we sampled the first 5 cm of the upper part of the siliceous surface boulders (gneiss, granite, pegmatite, sandstone) partly embedded in the alluvial deposit of the terrace and therefore not remobilized since their deposition (five and three sample were taken for dating T3 and T2, respectively).

Beryllium oxide targets were extracted following the chemical procedures of Brown et al. (1991) and Merchel and Herpers (1999). The extractions were made in the Cosmogenic Laboratory of Institut de Sciences de la Terre (ISTerre, France). ^{10}Be concentrations were measured at the accelerator mass spectrometry facility ASTER (CNRS, France) (Arnold et al., 2010). They were calibrated against NIST Standard Reference Material 4325 using its assumed ^{10}Be/^{9}Be ratio of $2.79 \pm 0.03 \times 10^{-11}$, and a ^{10}Be half-life of 1.387 ± 0.012 Ma (Chmeleff et al., 2010; Korschinek et al., 2010). Production rates were calculated following Stone (2000) using the modified scaling functions of Lal (1991) and a ^{10}Be production rate in quartz of 4.5 ± 0.3 at/g/a at sea level and high latitude. Geomorphic scaling factors were calculated following Dunne et al. (1999). All ^{10}Be age calculations were performed using attenuation lengths of 150, 1500 and 5300 g/cm^2 with associated relative contributions to the total production rate of 97.85%, 1.50% and 0.65% for neutrons, slow muons and fast muons, respectively (Braucher et al., 2003).

Methods and factors of correction for paleomagnetic effects remain a matter of debate and uncorrected ages do not significantly differ from intensity-corrected ages (e.g. Dunai, 2001; Carcaillet et al., 2004; Masarik et al., 2001; Pigati and Lifton, 2004), so in this study paleomagnetic intensity correction was not applied. Thus, numerical ages are given in ^{10}Be ka in order to allow straightforward correction for future refinements in production rates histories and paleomagnetic intensity corrections.

The incision rates were estimated from the ratio between the heights of the terrace surfaces above the current riverbed and the ^{10}Be exposure ages. These estimations were made in river terraces located sufficiently far from the deformation front not to suffer tectonic deformation (Figs. 2–4). In the lower reaches of the Santo Domingo river, the strath levels outcrop only in a few localized sites; thus, in order to homogenize the estimation of incision rates, the surfaces of the terraces were always taken as reference levels. The possible repercussions that this approach may generate in the estimation of the incision rate (e.g. overestimation) in the study area can be neglected for the following reasons: 1) the surfaces of the terraces have not been modified by post-depositional colluvia or tributary alluvial fan; 2) in most cases, the alluvial deposit is only few meters thick (Fig. 5a, b), which is negligible with respect to the incision of the terraces (more than 29 m, height of the lowest one); 3) the surfaces of the terraces are in general flat, which suggests that they have been little modified by denudation processes, or that the modifications have been uniform over the terrace surface (tread) (Fig. 5a); 4) in the few sites where strath levels can be observed, they are parallel to the surface of the corresponding terrace (Fig. 5a, b).

5. Geomorphic analysis and age calculations

5.1. General river description

The Santo Domingo river is located in the central part of the MA, and drains the Southeastern flank of the chain. Its catchment has a surface of 1250 km^2 upstream to Barinas city. Its source was glaciated during the Las Glacial Maximum (LGM) (Clarck et al., 2009), as suggested by well-preserved glacial features (e.g. Schubert and Vivas, 1993; Mahaney and Kalm, 1996; Carrillo, 2006). It flows over 200 km from the Mucubaji lake at 3570 m a.s.l. to the Apure river in the Llanos basin, with an outlet around 200 m a.s.l. The river in the upper reaches of the Santo Domingo flows from WSW to ENE for around 24 km along the Boconó fault and the axial part of the chain. In these reaches, the river flows over crystalline and metamorphic Paleozoic rocks (granite, gneiss and pegmatite) (Fig. 1c) (Hackley et al., 2005). Then it bends abruptly and flows from NW to SE downstream toward the front of the Southeastern flank. In this part, the river is orthogonal to the structural trend of the chain. It flows over crystalline-metamorphic Palaeozoic, calcareous Cretaceous, siliciclastic Neogene rocks and alluvial Quaternary alluvial sediments (Fig. 1c) (Hackley et al., 2005). The river crosses Quaternary faults, among which the POF and the SAFF, which belong to the Southeastern Foothills thrust system (Audemard et al., 2000; Audemard, 2009). In the lower reaches, the Santo Domingo river continues into the Llanos basin toward the Apure river, then into the Orinoco river, which reaches the Atlantic Ocean at more than 1500 km from the study area.

This work is geographically focused on the lower reach of Santo Domingo river, where river terraces have been studied since the first half of the XXth century (e.g. Liddle, 1928; Mackenzie, 1937; Pierce, 1960; Tricart and Millies-Lacroix, 1962; Zinck and Stagno, 1966). However, previous studies lack of detailed geomorphological analyses and numerical ages for these terraces. We therefore characterized terrace geometry (longitudinal and lateral extension, slope, height on the river, deposits thickness), stratigraphy, sedimentology, and dated their abandonment.

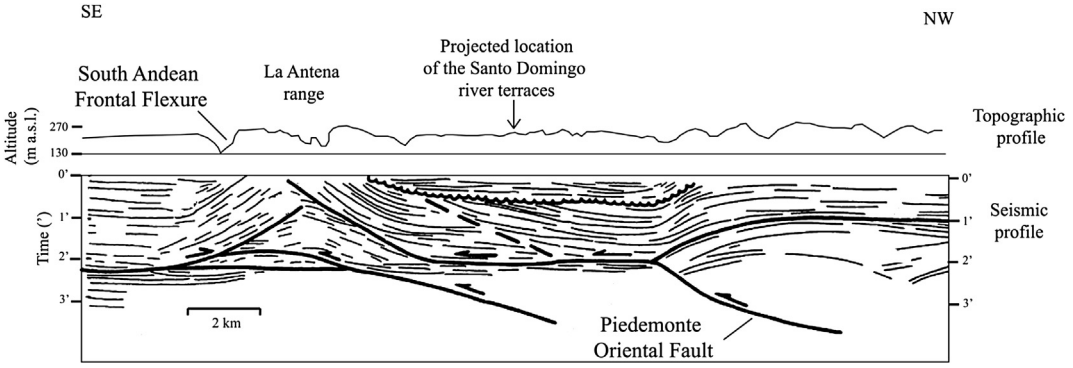

Fig. 2. Structural interpretation from seismic and topographic profiles across the Southeastern foothills of the MA (Funvisis, 1997; Duerto et al., 1998; Audemard, 1999). The faults exhibit ramp-flats geometry. Note the good matchinh between subsurface (seimic data) and surface deformation (topographic data). In the middle part of the section, the geometry of the Piedemonte Oriental Fault (POF) (low-dipping fault plane) causes a rising almost horizontally of the ground surface of his hangingwall block, where the river terraces located in the lower reaches of Santo Domingo river (object of this study and projected in this section) are located. In this part of the section, the POF has not produced surface deformation. Location of this section is shown in Fig. 1.

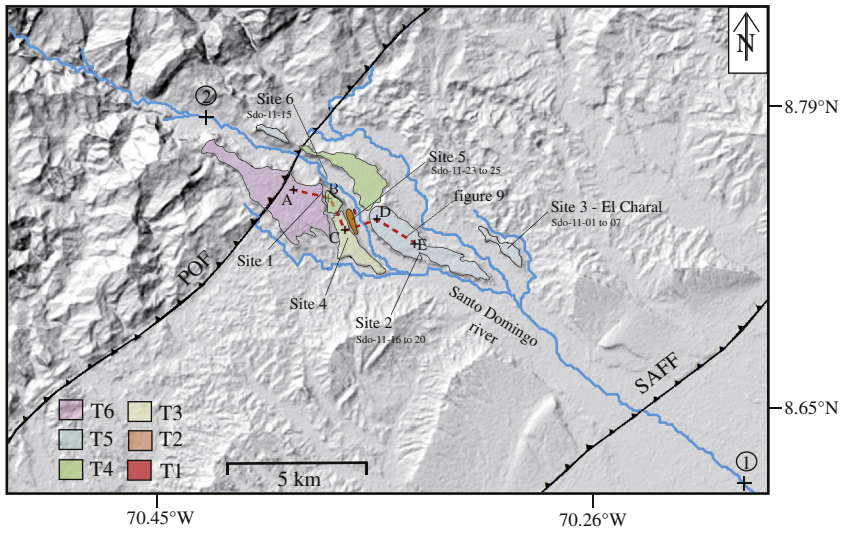

Fig. 3. Geomorphologic map of the lower Santo Domingo river. Surface projection of the POF and SAFF location are based on Audemard et al. (2000). Longitudinal river profile of the Fig. 4 was constructed in the lower reaches of the river between the point 1 and 2. The studied sites and the sampling locations are also shown. Location of the Fig. 9 is shown with red dashed line. (For interpretation of the references to colour in this figure legend, the reader is referred to the web version of this article.)

5.2. Terrace geometry

On the basis of geomorphic and stratigraphical analysis, six well preserved strath terraces were mapped in the lower reaches of the Santo Domingo river between Barinitas city and El Charal villages (Figs. 3 and 4). These terraces are called in the following T6 to T1, from the oldest to the youngest. They have an average downstream slope between 1.1° and 0.4°, decreasing with age of the terrace and downstream. Average slope of the present riverbed is 0.4° (Fig. 4). In general, the alluvial deposits of the terraces overlay detritic poorly lithified Neogene rocks (conglomerate, sandstone or mudstone), and their stratigraphy is relatively similar. Alluvial deposits present a lower unit of fine gravelled sand matrix supported conglomerate, where the clasts are composed of stratified well-rounded pebbles and cobbles (2–10 m thick), deposited in a fluvial environment. The clasts are constituted mainly of gneiss, granite and sandstones. This unit is overlain by a fine alluvial sand and clay unit that represented floodplain facies (50–150 cm thick).

All the river terraces analysed in this study are located sufficiently far from the deformation front not to suffer tectonic deformation. Moreover, most of the terraces are in the same structural block, except T6, which is traversed by the inferred projection of the POF (Fig. 2) (Audemard et al., 2000). Nevertheless, this fault has not produced surface deformation since the abandonment of T6, as proven by the absence of fault scarp at the surface of this terrace (Fig. 4). Therefore, no local structural control except at the front exists over the fluvial incision. The flat surface of the terraces when they cross two different lithological bedrock units and the absence of knickpoint in the current longitudinal river profile (Fig. 4) suggest that the fluvial incision is not dependent on

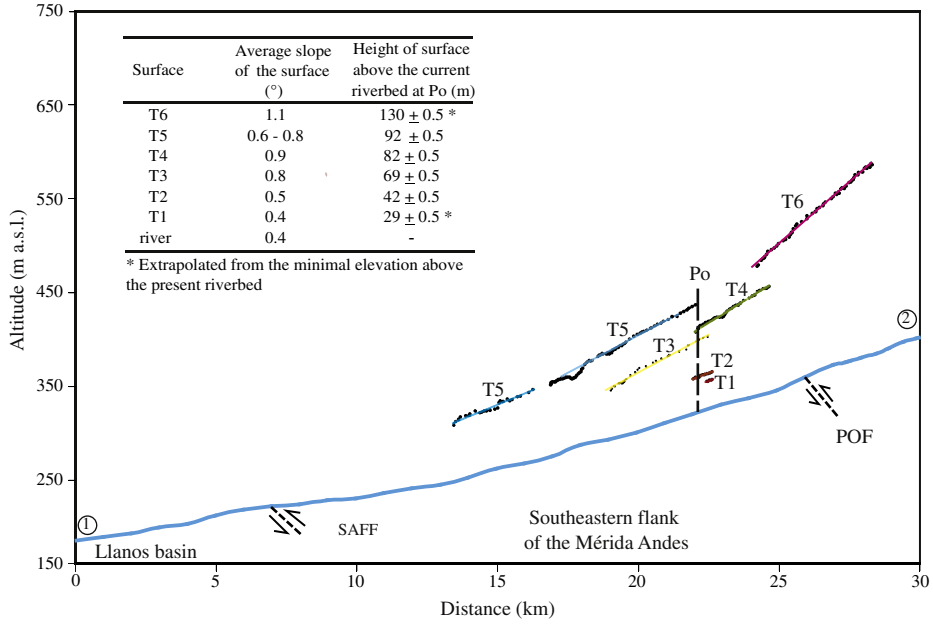

Fig. 4. Longitudinal profiles of the lower Santo Domingo river and terraces. The table in the upper left corner summarizes the geometry of the terraces. The localization of Po is shown in the figure. The height of the terraces T6 and T1 above the current riverbed at Po, were extrapolated from the minimal elevation of these terraces. Location of the POF and SAFF are based on Audemard et al. (2000).

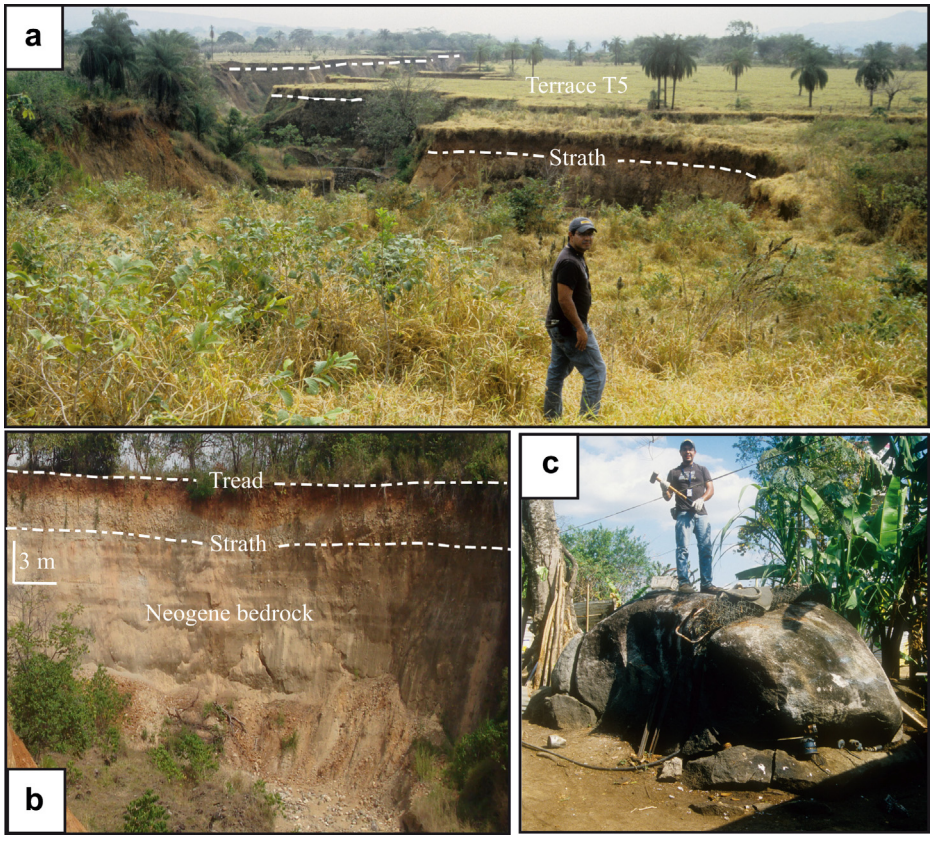

Fig. 5. Morphology of river terraces in the study area. **a**) Flat surface of the terrace T5 (site 2). **b**) Alluvial deposit of T5 composed of a basal unit of stratified cobbles and pebbles and an upper unit of red sand and silt. This deposit cut the sandstone Neogene bedrock. The surface of the terrace is parallel to the strath surface (site 2). **c**) Plurimetric rounded boulder partially embedded into the alluvial deposit of terrace T3 (site 4). Pictures by R. Vassallo (a, c) and M. Alvarado (b).

the lithology of Neogene bedrock. The effect of the growth of the drainage network over the fluvial incision is evidenced by the longitudinal upstream incision increase, which produces vertically divergent terraces upstream (Fig. 4). This effect is therefore lowest toward the outlet of the catchment. In order to minimize and homogenize this effect, we evaluate the fluvial incision at a single point (Po in the text) of the current riverbed in the lower part of the catchment, where most of the terraces are present (Fig. 4). Consequently, the long term fluvial incision rate in the lower reach of the Santo Domingo river is mainly controlled by mountain uplift. Hence the quantification of the incision rate allows the estimation of the uplift rate for the Southeastern flank of the MA.

In the following, we discuss the individual geometry and stratigraphy-sedimentology of the terraces. T6 is a river terrace located on the right bank of the Santo Domingo river, on which the city of Barinitas has settled (Fig. 6). The surface of this terrace has an average downstream slope of 1.1°. This terrace, as well as the other terraces, has a higher slope than the current riverbed (Fig. 4). The development of Barinitas city on the terrace inhibits the characterization of the original surface and the alluvial deposit. However, in a natural section located toward the Southern border of the terrace (site 1 – Figs. 3 and 6), T6 has an irregular surface with a mean rugosity around 50 cm. In this site the alluvial deposit of T6 is made of a gravel-sand matrix supported conglomerate. The clasts are composed by stratified rounded pebbles and cobbles (~400 cm thick).

Terrace T5 was studied at two sites along the study area. Despite this terrace is largely used for agriculture, there are places where the original surface of the terrace is well preserved. The surface of T5 is mainly flat with a variable downstream slope between 0.8° and 0.6° (Fig. 5a). At site 2 (Figs. 3 and 6), the alluvial deposit of T5 is around 4 m thick. It contains a basal unit of stratified rounded pebbles and cobbles. Thickness of the basal unit varies laterally (in a context of fluvial channels and bars sedimentation) from 0 to 350 cm, and is overlain by a red sand unit, which is 50–400 cm thick. At this site, the alluvial deposit of T5 is above a strath surface, located at the top of the sandstone Neogene bedrock (Fig. 5b).

T5 was also studied, in a pit-soil of 2 × 3 × 2 m located to the Southeast of the studied area (site 3 – Fig. 3). At this site, the surface of the terrace is relatively flat, with a maximal rugosity around 10 cm. The lower unit of the alluvial deposit of T5 is a 150 cm thick roughly stratified bed. This unit contains well-rounded pebbles and cobbles. An intermediate unit of 10 cm is made of coarse sand. The upper unit shows 40 cm of unsorted fine sand, silt and clay (Fig. 7).

Terrace T4 was observed on both banks of the river (Figs. 3 and 6). On the left bank, T4 is better preserved. T4 has a flat surface with an average downstream slope of 0.9° (Fig. 4). The alluvial deposit of T4 comprises a lower unit of stratified rounded pebbles and cobbles, which is at least 10 m thick. An upper thin ~60 cm thick sandy unit is observed.

T3 is preserved on the right bank of the river (Figs. 3 and 6). The surface of terrace T3 is mainly flat with an average downstream slope of 0.8° (Fig. 3). The alluvial deposit of T3 exhibits a lower unit of stratified well-rounded pebbles and cobbles at least 100 cm thick, and an upper thin fine sand and clay unit, not thicker than ~70 cm. Additionally, plurimetric rounded boulders composed of crystalline rocks, with an average diameter of ~200 cm and a maximal size of 400 cm, are embedded into the alluvial material. The top of these boulders are exposed >100 cm above ground surface (Fig. 5c).

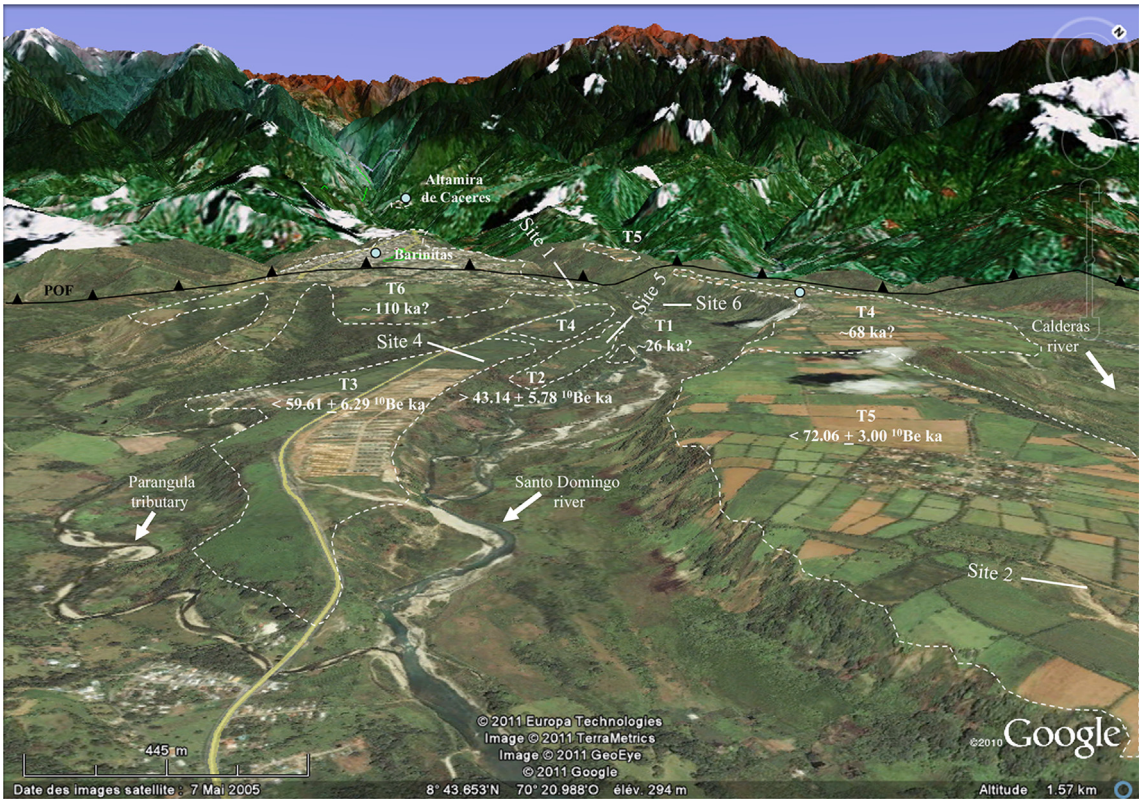

Fig. 6. Panoramic view of terraces from satellites images (Google earth, 2005). The estimated and extrapolated ages calculated in the present study are assigned to the terraces. The studied sites are also shown. Surface projection of the POF location are based on Audemard et al. (2000).

Terraces T2 and T1 are located on the right bank of the river. These terraces are the lowest and smallest preserved terraces in the study area (Figs. 3 and 6). The surfaces of these terraces are roughly irregular, with a rugosity that can reach 30 cm. They have a downstream slope of 0.5° (T2) and 0.4° (T1) (Fig. 5). The alluvial deposit of both terraces contains a lower unit of ~100 cm thick of stratified well-rounded pebbles and cobbles, and a ~150 cm thick upper unit of fine sand and clay. Into this unit, few pluri-decimetric exposed boulders, with an average diameter of 40 cm can be found.

5.3. Age calculations

In order to determine the exposure ages of the terraces identified in the lower reaches of the Santo Domingo river, the concentrations of ^{10}Be in samples taken in terraces T5, T3 and T2 were analysed. The results are discussed from oldest to youngest.

Terrace T5 was sampled at site 3 (Fig. 3). A cosmogenic depth profile was made along a 200 cm deep pit-soil (Fig. 7). At the sampling site, the small roughness of the surface of T5 suggests that

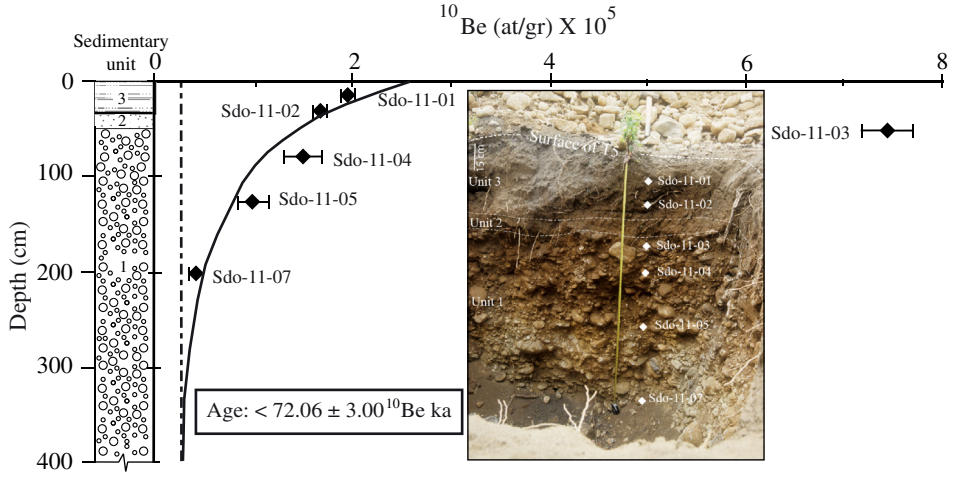

Fig. 7. Depth profile of the ^{10}Be concentration within the alluvial deposit of the terrace T5 at site 3. The depth-production best fit using a chi-square inversion is in solid line. The dashed line shows the inherited ^{10}Be concentration. Details of the exposure age calculations are in Table 1. On the picture we can see the soft rugosity in the surface of terrace T5 and the stratigraphy of the alluvial deposit. It is composed of three units. Unit 1: roughly stratified well-rounded pebbles and cobbles. Unit 2: coarse sand. Unit 3: fine sand, silts and clay. Picture by R. Vassallo.

a denudation process could have only slightly modified the original surface of the terrace. The local loss of alluvial material probably does not exceed the maximum rugosity of the surface irregularities (~10 cm). This upper-bound value was taken into account for the data inversion to determine a maximum age (Arboleya et al., 2008; Schmidt et al., 2011). The four lower samples are individual cobbles, coming from the coarse unit (see Section 5.2). The two other samples are constituted of fine sand from the upper unit (Fig. 7). The distribution of ^{10}Be concentration shows an exponential decrease with depth, except for the sample Sdo-11-03 (Fig. 7). This sample shows a high grade of weathering with respect to the other samples with similar lithology, and suggests a longer pre-exposure history. Thus, this sample was not considered for the age estimation. A mathematical model was used, in order to estimate the ^{10}Be in surface and consequently the exposure age of the terrace T5. Using a chi-square inversion to minimize the difference between observed and modeled ^{10}Be data (e.g. Braucher et al., 2003; Ritz et al., 2006) and assuming a density of 2.4 g/cm^3, the maximum inherited concentration was estimated at 0.30 ± 0.03 × 10^5 at/g (Fig. 7). This value is consistent with the inherited component estimated from the sediments of the active stream (Sdo-11-15 – Table 1). This result yields a maximum exposure age of 72.06 ± 3.00 ^{10}Be ka (Table 1).

To date terrace T3, five samples were taken from the pluri-metric boulders partially embedded into the alluvial deposit of the terrace (Sdo-11-16 to 20 – Table 1) (see Section 5.2). ^{10}Be concentrations are similar and range between 2.14 ± 0.12 and 2.51 ± 0.20 × 10^5 at/g (Table 1). The height of the boulder tops above ground surface of the terrace (some of them >80 cm) suggests that the samples have not been shielded by any matrix even if a slight denudation of the surface of the terrace occurred. Despite the difficulty to know the amount of inheritance in each boulder, the fact that these boulders are only present in terrace T3 and their homogeneous ^{10}Be concentrations suggest that these boulders have a similar simple and short pre-exposure history. This assumption gives a maximum exposure age estimate for this terrace that cluster around 59 and 70 ka. Therefore, the apparent age given by the boulder with the smallest concentration should be the closest to the true age (Vassallo et al., 2011). Sample Sdo-11-16 is the one with the lowest concentration with 2.14 ± 0.12 × 10^5 at/g, and yields a maximum exposure age of 59.21 ± 6.29 ^{10}Be ka (Table 1).

For terrace T2, we applied the same strategy used for terrace T3. Three surface samples were taken from pluri-decimetric well-rounded boulders, which outcrop at different heights above the ground. Two of them have similar ^{10}Be concentration (Sdo-11-23 and Sdo-11-25 – Table 1). At the sampling site, the surface of T2 has an irregular slope toward the axis of the valley, which suggests a bad preservation of the original surface. Therefore the samples could have suffered shielding since deposition. In this case, it is also difficult to know the amount of inheritance in each boulder. However, the impact in the estimation of the age that could be caused by the loss of thickness of this terrace of at least 30 cm (maximum rugosity of the surface –see subsection 5.2), is likely higher than the impact caused by the amount of inheritance. Therefore, we use the highest concentration for the age estimation, which corresponds to a minimum value. Sample Sdo-11-23 is the one with the highest concentration with 1.53 ± 0.15 × 10^5 at/g, which yields a minimum age of 43.14 ± 5.78 ^{10}Be ka (Table 1).

Table 1
Results of the ^{10}Be analysis. Calibration against NIST Standard Reference Material 4325. ^{10}Be concentrations uncertainties include analytical errors from the counting statistics and blank correction, whereas the ages uncertainties also include the errors of the production rate introduced by the scaling model of Lal (1991) – Stone (2000) and the errors of the ^{10}Be decay constant (Chmeleff et al., 2010; Korschinek et al., 2010). (*) Age estimated from ^{10}Be depth profile assuming a maximum erosion of 10 cm and a density of 2.4 g/cm^3.

Sample	Type of sample	Lithology	Latitude (N)	Longitude (E)	Altitude (m a.s.l.)	depth (cm)	Height above the ground (cm)	Surface P_0 (at/g/y)	Shielding factor	^{10}Be concentration (10^5 at/g)	^{10}Be age (ka)	Terrace
Site 3 – El Charal			−70.2903	8.7302	321			3.50 ± 0.23	1			T5
Sdo-11-01	Sand	Heterogeneous				15				1.95 ± 0.10	72.06 ± 3.00*	
Sdo-11-02	Sand	Heterogeneous				30				1.66 ± 0.10		
Sdo-11-03	Cobble	Gneiss				53				7.44 ± 0.39		
Sdo-11-04	Cobble	Granite				80				1.49 ± 0.21		
Sdo-11-05	Cobble	Gneiss				125				0.97 ± 0.17		
Sdo-11-07	Cobble	Granite				200				0.39 ± 0.06		
Site 4 – Santo Domingo			−70.3696	8.738	380			3.66 ± 0.24	1			T3
Sdo-11-16	Metric boulder	Pegmatite					70			2.14 ± 0.12	59.61 ± 6.29	
Sdo-11-17	Metric boulder	Granite					50			2.52 ± 0.08	70.18 ± 6.71	
Sdo-11-18	Metric boulder	Granite					40			2.51 ± 0.20	70.08 ± 8.37	
Sdo-11-19	Metric boulder	Granite					86			2.45 ± 0.13	68.33 ± 7.19	
Sdo-11-20	Metric boulder	Granite					180			2.34 ± 0.15	65.18 ± 7.28	
Site 5 – Los Platanos			−70.3711	8.7486	361			3.60 ± 0.24	1			T2
Sdo-11-23	Pluri-centimetric boulder	Sandstone					15			1.53 ± 0.15	43.14 ± 5.78	
Sdo-11-24	Pluri-centimetric boulder	Granite					8			0.82 ± 0.05	23.14 ± 2.60	
Sdo-11-25	Pluri-centimetric boulder	Sandstone					15			1.43 ± 0.07	40.17 ± 4.13	
Site 6 – Barinesa bridge			−70.389	8.7701	348							
Sdo-11-15	Sand	Heterogeneous					0			0.32 ± 0.02		river

6. Discussion

6.1. Incision rates and tectonic uplift

The incision rates were estimated for terraces T5, T3 and T2 at a single point (Po in Fig. 4), where most of the terraces are present. The results are summarized in the Table 2.

These estimations allow concluding that the long-term incision rate close to the mountain front in the lower Santo Domingo river averages around 1.1 mm/a over the last 70 ka. Taking into account the geologic and geomorphologic setting of the study area (see subsection 5.2.), this incision rate represents the uplift rate of the Southeastern flank of the MA. This estimation of the uplift rate is in the same range of the recent estimation ($\sim 1.7 \pm 0.7$ mm/a) done by Wesnousky et al. (2012) for the Northwestern flank over the Late Pleistocene. Additionally, this value is similar to the exhumation rate of 0.8 mm/a for the last 800 ka, proposed by Kohn et al. (1984) from cooling ages derived from apatite fission track of samples located in El Carmen Block, in the central part of the MA (Fig. 1). These results give a more detailed and broader picture of the uplift rate of the MA. In fact, they seem to indicate that the two flanks of the MA (NE and SW) uplift at a similar rate and that this rate is probably unchanged over several 100 ka. Nonetheless a more extensive analysis and dating of river terraces located in the valleys along the axis of the chain (e.g. Chama, Upper Santo Domingo, Upper Mocotíes and Pueblo Llano valleys), as well as in the Northwestern and Southeastern flanks (e.g. Lower Motatán, Guanare, Escalante and Uribante valleys) are required to constrain the spatial distribution of the uplift rate of the chain.

6.2. Terrace formation vs climate

From the extrapolation of the average incision rate performed in this study (~ 1.1 mm/a) and the height of the terraces at Po above the current riverbed, the ages of terraces T6, T4 and T1 were estimated at around 110, 68 and 26 ka, respectively (Fig. 8, Table 2). These results coupled with the exposure ages directly estimated for T5, T3 and T2 (see subsection 5.3) show that the process of terraces formation in the lower reach of Santo Domingo river occurred at a much higher frequency than an interglacial/glacial cycle (10^4–10^5 years) (Fig. 9).

Our dating also shows that all of the terraces younger than Early Mérida Glaciation in the lower Santo Domingo river were formed during the El Pedregal Interstade (between ~ 65 and 22 ka). During this period the climatic conditions were relatively warm and humid (Dirszowsky et al., 2005; Rull, 2005; Kalm and Mahaney, 2011). The comparison of our dating with the high resolution paleoclimatic record of the Cariaco basin (Peterson et al., 2000; González et al., 2008), show a correlation between the ages of abandonment of terraces T5, T3 and T2 and short periods of cold and dry conditions around 74, 60 and 43 ka (i.e. stadial (S) and Heinrich event (H6) conditions – Fig. 10). Therefore this correlation shows that the abandonment of the terraces occurred during a long-term warm and humid stage, but was triggered by short and rapid climatic variations from warm to cold conditions (Fig. 10). Hence, we argue that the process of river terraces formation in the lower reaches of Santo Domingo river was probably controlled by climatic variations. During the warm and humid periods of the El Pedregal Interstade (Dirszowsky et al., 2005; Rull, 2005; Kalm and Mahaney, 2011) the river attained an equilibrium between incision and aggradation. Consequently strath surfaces were developed. Then, during short period of cold and dry conditions equilibrium was interrupted by vertical fluvial incision triggered by the decrease in the transport capacity. Additionally, the signature of an instantaneous high energy aggradations event is put in evidence by the presence of the pluri-metric boulders at the surface of terrace T3. These boulders are embedded into the alluvial deposits and were probably transported and deposited by debris flow climatically or tectonically triggered in a context of high water discharge and sediment supply. In the case of climate controlled events, these events could have been similar to those occurring today in the Mérida Andes (Olivero et al., 2005a,b).

This climatic-driven formation model is opposed to the glacial/interglacial model previously proposed for the terraces of MA by Tricart and Millies-Lacroix (1962) (published well before that the recent advance in Quaternary geochronology and paleoclimatology) that associated the abandonment of the terraces to interglacial conditions. Our results show that this model is not applicable in the lower reaches of the Santo Domingo river. In fact, no river terraces have been formed in the study area during the end of the maximum extension of ice sheets through the Last Glacial period (LGM; Clark et al., 2009), which is well documented in glacial sediments in the core of the MA and dated at 21.5 ka (Kalm and Mahaney, 2011). This comparison also suggests that the process of terraces formation could be different in the upper catchment of the river. Thus, an analysis of river terraces in the upper part of the Santo Domingo catchment, close to the interaction with glacial fluctuations, could allow a better understanding of this issue.

Table 2
Summary of Santo Domingo river terraces ages and incision rates. The extrapolated ages for the terraces T6, T4 and T1 are also shown. Details of the extrapolated age calculations are in subsection 5.2.

Terrace	Height of surface above the current riverbed at Po (m)	Exposure age (ka)	Extrapolated age (ka)	Incision rate at Po (mm/a)
T6	130 ± 0.5[a]	–	110	–
T5	92 ± 0.5	72.06 ± 3.00	–	1.27 ± 0.06
T4	82 ± 0.5	–	68	–
T3	69 ± 0.5	59.61 ± 6.29	–	1.16 ± 0.12
T2	42 ± 0.5	43.14 ± 5.78	–	0.98 ± 0.13
T1	29 ± 0.5*	–	26	–

[a] Extrapolated from the minimal elevation above the current riverbed.

7. Conclusion

This study established a river terrace chronology based on cosmogenic ages for the lower reaches of the Santo Domingo river. The six well-preserved Late Pleistocene strath terraces identified allowed reconstructing the history and the dynamics of the incision as a response to climatic and tectonic inputs.

We estimated maximum exposure ages for terraces T5 and T3 at 72.06 ± 3.00 and 59.61 ± 6.29 ^{10}Be ka, respectively, and a minimum

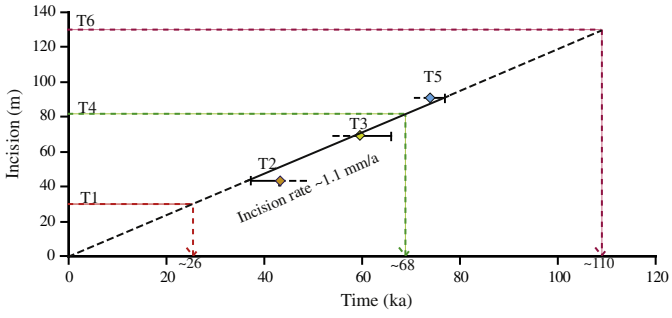

Fig. 8. Incision rate of lower Santo Domingo reaches calculated from the ratio between the height of terraces T5, T3 and T2 and the exposure ages estimated in this work. Extrapolated ages for T6, T4 and T1 were estimated assuming a constant incision rate over the last 120 ka. Maximum and minimum ages performed are plotted with their uncertainty associated and a dashed line toward younger and older times (maximum and minimum ages, respectively).

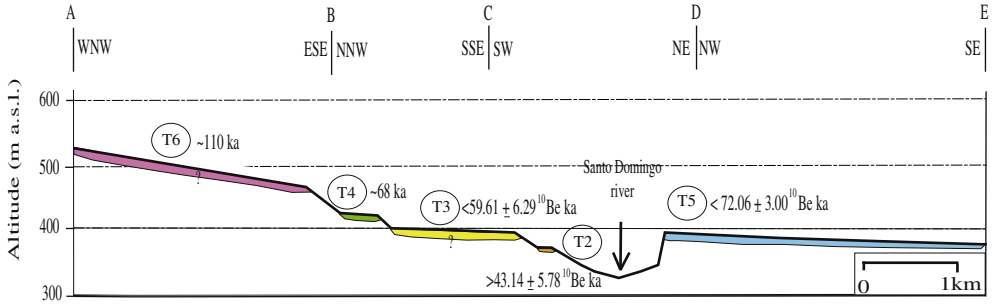

Fig. 9. Cross section trough the river terraces of the lower reaches of the Santo Domingo river. The ages of the terraces correspond to the numerical ages and extrapolation ages proposed in this work. Red-dashed line in Fig. 3 indicates location of this profile. Note that T5, on the left bank, is located downstream with respect to the other terraces.

exposure age for terrace T2 at 43.14 ± 5.78 ^{10}Be ka. These results and the elevations of terraces above the present riverbed yield a long-term constant incision rate around 1.1 mm/a over the last 70 ka.

The analysis of the geologic and geomorphologic setting allowed proposing that the long-term fluvial incision in the lower Santo Domingo river is mainly controlled by mountain uplift. Therefore we consider that the value estimated for the incision rate (~1.1 mm/a) can be converted into the Late Pleistocene uplift rate of the Southeastern flank of the MA. This value is in the same range of the uplift rate on the same period of the Northwestern flank (Wesnousky et al., 2012), showing that the MA may be being symmetrically uplifting on both flanks.

From the extrapolation of the long-term average incision rate estimated in this study, the ages of the terraces T6, T4 and T1 were estimated at around 110, 68 and 26 ka, respectively. This result shows that the process of terraces formation on the Southeastern flank of the MA occurred with a higher frequency than a glacial/interglacial cycle. In particular terraces seem to have been abandoned during warm to cold transitions and are therefore climatically controlled. However, the impact of the climatic input in terraces formation remains to be quantified, while other parameters such as seismic activity within the MA could play a significant role.

Acknowledgments

The authors thank the Fondo Nacional de Ciencia, Tecnología e Innovación – Venezuela (FONACIT) and the Fundación Gran

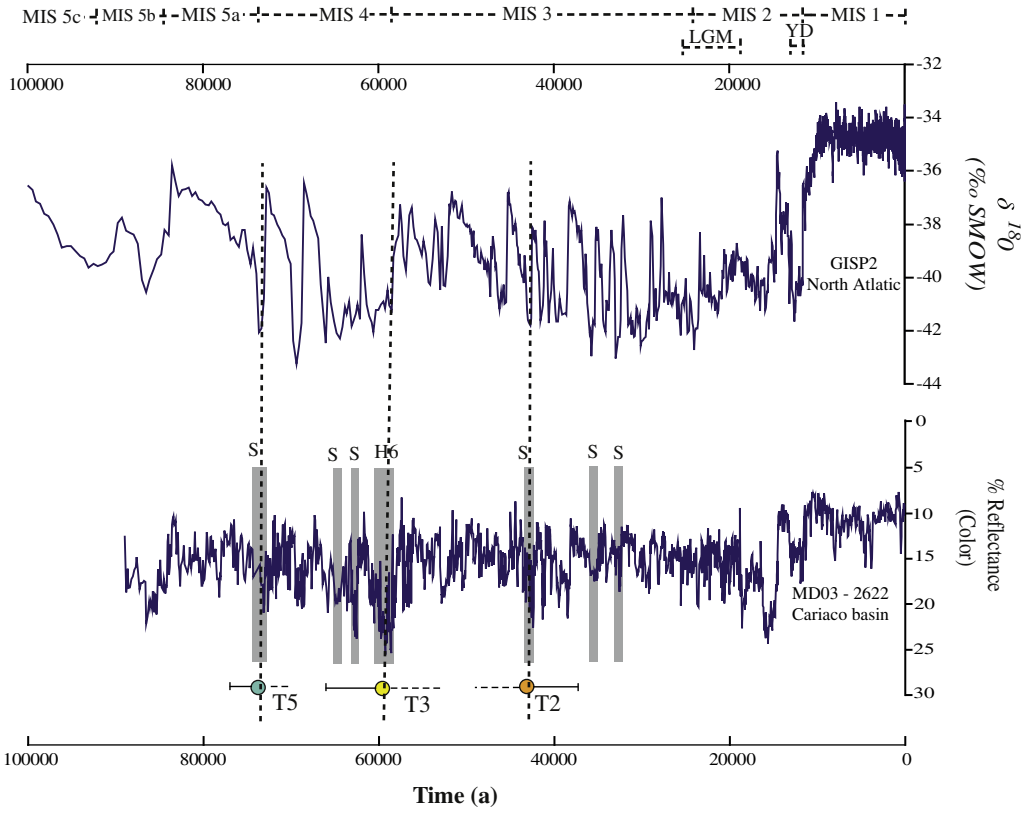

Fig. 10. Comparison of ages of abandonment of the lower Santo Domingo river terraces with: **a**) δ^{18}O record from the GISP2 ice core (Grootes et al., 1993; Stuiver et al., 1995). **b**) Color reflectance curve of Cariaco basin (Peterson et al., 2000). The gray rectangles represent short periods of cold and dry conditions identified by Peterson et al. (2000) and González et al. (2008) in the Cariaco basin. (S) stadial. (H6) Heinrich event 6. (MIS) Marine Isotope stage (Aitken and Stokes, 1997; Wright, 2000; Shackleton 1987); (LGM) Last Glacial Maximum (Clark et al., 2009); (YD) Younger Dryas (Berger, 1990).

Mariscal de Ayacucho by funded otorgated through the ECOS Nord project PI-2007001823 to O.G. and R.V. during field work. We also thank the Fundación Venezolana de Investigaciones Sismológicas (FUNVISIS) by the aerial photos and topographic maps of the study area, and the logistical support given during the field work. We thank the Fundación Instituto de Ingeniería – Laboratorio de Procesamieno Avanzado de Imagenes Satelitales – LPAIS – of Venezuela by supporting in construction of the DEM of the study area. We thank the Aster team (Mrs. Arnold M., Aumaitre, G. and Keddadouche, K.) for the isotopic mesures of the samples. This publication was also made possible through support provided by the IRD-DPF to O.G. We thank V. regard and an anonymous reviewer for their constructive comments that allowed us to significantly improve the quality of the paper.

References

Aitken, M.J., Stokes, S., 1997. Chapter 1. In: Taylor, R.E., Aitken, M.J. (Eds.), Chronometric Dating in Archaeology. Birkhäuser, ISBN 0-306-45715-6. ISBN 978-0-306-45715-9, google books.

Anderson, R.S., Repka, J.L., Dick, G.S., 1996. Explicit treatment of inheritance in dating depositional surfaces using *in situ* ^{10}Be and 26Al. Geology 24, 47–51.

Antoine, P., Limondin, N.L., Chaussé, C., Lautridou, J.-P., Pastrea, J.-F., Auguste, P., Bahaine, J.-J., Falguères, C., Galehb, B., 2007. Pleistocene fluvial terraces from Northern France (Seine, Yonne, Somme): synthesis, and new results from interglacial deposits. Quat. Sci. Rev. 26, 2701–2723.

Arboleya, M.-L., Babault, J., Owen, L., Teixell, A., Finkel, R., 2008. Timing and nature of quaternary fluvial incision in the Ouarzazate foreland basin, Morocco. J. Geol. Soc. 165, 1059–1073.

Arnold, M., Merchel, S., Bourles, D., Braucher, R., Benedetti, L., Finkel, R.C., Aumaitre, G., Gottdang, A., Klein, M., 2010. The French accelerator mass spectrometry facility ASTER: Improved performance and developments. Nucl. Instrum. Methods Phys. Res. Sect. B: Beam Interac. Mater. Atoms 268, 1954–1959.

Audemard, F.A., 1999. Morpho-structural expression of active thrust fault systems in humid tropical foothills of Colombia and Venezuela. Z. für Geomorphologie 118, 1–8.

Audemard, F.A., 2003. Geomorphic and geologic evidence of ongoing uplift and deformation in the Mérida Andes, Venezuela. Quat. Int. 101–102, 43–65.

Audemard, F.A., 2009. Flexura Frontal sub-andina, Venezuela (VE-07). In: Servicio Nacional de Geología y Minería (Ed.), Atlas de las deformaciones cuaternarias de Los Andes, Proyecto multinacional andino: Geociencia para las comunidades andinas, pp. 300–311. Publicacion Geológica nacional N° 7.

Audemard, F.A., Machette, M., Cox, J., Dart, R., Haller, K., 2000. Map and Database of Quaternary Faults in Venezuela and Its Offshore Regions. US Geological Survey Open-File Report 00-0018. Include map at scale 1:2,000,000 and 78-page report.

Audemard, F.E., Audemard, F.A., 2002. Structure of the Mérida Andes, Venezuela: relations with the South America-Caribbean geodynamic interaction. Tectonophysics 345, 299–327.

Backé, G., Dhont, D., Hervouët, Y., 2006. Spatial and temporal relationships between compression, strike–slip and extension in the Central Venezuelan Andes: clues for Plio–Quaternary tectonic escape. Tectonophysics 425, 25–53.

Berger, W.H., 1990. The Younger Dryas cold spell – a quest for causes. Glob. Planet. Change 3 (3), 219–237.

Bermúdez, M., 2009. Cenozoic Exhumation Patterns across the Venezuelan Andes: Insights from Fission-track Thermochronology. Ph.D. thesis. Joseph Fourier University, France, p. 305.

Bermúdez, M., van der Beek, P., Bernet, M., 2011. Asynchronous Miocene-Pliocene exhumation of the central Venezuelan Andes. Geology 39 (2), 139–142.

Braucher, R., Brown, E.T., Bourlès, D.L., Colin, F., 2003. *In situ* produced ^{10}Be measurements at great depths: implications for production rates by fast muons. Earth Planet. Sci. Lett. 211, 251–258.

Brown, E.T., Edmond, J.M., Raisbeck, G.M., Yiou, F., Kurtz, M.D., Brook, E.J., 1991. Examination of surface exposure ages of moraines in Arena Valley, Antarctica, using *in situ* produced ^{10}Be and ^{26}Al. Geochim. Cosmochim. Acta 55, 2269–2283.

Carcaillet, J., Bourlès, D.L., Thouveny, N., 2004. Geomagnetic dipole moment and ^{10}Be production rate intercalibration from authigenic ^{10}Be/^{9}Be for the last 1.3 Ma. Geochem. Geophys. Geosystem. 5. http://dx.doi.org/10.1029/2003GC000641.

Carrillo, E., 2006. L'Enregistrement sédimentaire de la sismicité récente le long de la frontière sudoccidentale de la plaque caraïbe 'Faille de Boconó): Modalités et chronologie. Contribution à l'estimation de l'aléa sismique régional. Ph.D. thesis. Université de Savoie, France, p. 335.

Chmeleff, J., Von Blanckenburg, F., Kossert, K., Jakob, D., 2010. Determination of the ^{10}Be half-life by multicollector ICP-MS and liquid scintillation counting. Nucl. Instruments Methods Phys. Res. Sect. B: Beam Interac. Mater. Atoms 268, 192–199.

Clark, Peter U., Dyke, Arthur S., Shakun, Jeremy D., Carlson, Anders E., Clark, Jorie, Wohlfarth, Barbara, Mitrovica, Jerry X., Hostetler, Steven W., 2009. The last glacial maximum. Science 325 (5941), 710–714.

Colletta, B., Roure, F., De Toni, B., Loureiro, D., Passalacqua, H., Gou, Y., 1997. Tectonic inheritance, crustal architecture, and contrasting structural styles in the Venezuelan Andes. Tectonics 16 (5), 777–794.

Colmenares, L., Zoback, M.D., 2003. Stress field and seismotectonics of Northern South America. Geology 31, 721–724.

Corredor, F., 2003. Eastward extent of the Late Eocene-Early Oligocene onset of deformation across the Northern Andes: constraints from the Northern portion of the Eastern Cordillera fold belt, Colombia. J. South Am. Earth Sci. 16, 445–457.

Cortés, M., Angelier, J., 2005. Current states of stress in the Northern Andes as indicated by focal mechanisms of earthquakes. Tectonophysics 403, 29–58.

Dansgaard, W., Johnsen, S.J., Clausen, H.B., Dahl-Jensen, N.S., Gundestrup, N.S., Hammer, C.U., Hvidberg, C.S., Steffensen, J.P., Sveinbjörnsdottir, A.E., Jouzel, J., Bond, J., 1993. Evidence for general instability of past climate from a 250-kyr ice-core record. Nature 364, 218–220.

De Toni, B., Kellogg, J., 1993. Seismic evidence for blind thrusting of the Northwestern flank of the Venezuelan Andes. Tectonics 12 (6), 1393–1409.

Dhont, D., Backé, G., Hervouët, Y., 2005. Plio–Quaternary extension in the Venezuelan Andes: mapping from SAR JERS imagery. Tectonophysics 399, 293–312.

Dirección de Cartografía Nacional, 1976. Mapas Topograficos a Escala 1:25000. Hojas, Barinitas, Rio Calderas, Qda. Seca, Campo Azul, La yuca.

Dirszowsky, R.W., Mahaney, W.C., Hodder, K.R., Milner, M.W., Kalm, V., Bezada, M., Beukens, R.P., 2005. Lithostratigraphy of the Mérida (Wisconsinan) glaciation and Pedregal interstade, Mérida Andes, NorthwesternVenezuela. J. South Am. Earth Sci. 19, 525–536.

Duerto, L., Audemard, F.E., Lugo, J., Ostos, M., 1998. Síntesis de las principales zonas triangulares en los frentes de montana del occidente venezolano. In: IX Congreso Venezolano de Geofisica (CDRom; paper # 25).

Dunai, T.J., 2001. Influence of secular variation of the geomagnetic field on production rates of *in situ* produced cosmogenic nuclides. Earth Planet. Sci. Lett. 193, 197–212.

Dunne, J., Elmore, D., Muzikar, P., 1999. Scaling factors for the rates of production of cosmogenic nuclides for geometric shielding and attenuation at depth on sloped surfaces. Geomorphology 27, 3–11.

Funvisis, 1997. Estudio neotectónico y geología de fallas activas en el piedemonte surandino de los Andes venezolanos (Proyecto INTEVEP 95–061). unpublished report for INTEVEP, S.A. Funvisis', p. 155. ± appendices.

Giegengack, R., 1984. Late Cenozoic tectonic environments of the central Venezuelan Andes. In: Bonini, W., Hargraves, R., Shagam, R. (Eds.), The Caribbean-south American Plate Boundary and Regional Tectonics, Memoir – Geological Soc. of America, vol. 162, pp. 343–364.

González, C., Dupont, L.M., Behling, H., Wefer, G., 2008. Neotropical vegetation response to rapid climate changes during the last glacial: palynological evidence from the Cariaco basin. Quat. Res. 69, 217–230.

Google earth V 6.1.0.5001, Mai 7, 2005. Barinitas City, Mérida Andes. 8° 43.653'N, 70° 20.988'W, Eye Alt 1.57 Km. SIO, NOAA, U.S. Navy, NGA, GEBCO. GeoEye. http://www.googleearth.com.

Grootes, P.M., Stuiver, M., White, J., Johnson, S., Jouzel, J., 1993. Comparison of oxygen isotope records from the GISP2 and GRIP Greenland ice cores. Nature 366, 552–554.

Hackley, P.C., Urbani, F., Karlsen, A.W., Garrity, C.P., 2005. Geologic Shaded Relief Map of Venezuela. U.S. Geological Survey Open File Report 2005–1038.

Hancock, G.S., Anderson, R.S., Chadwick, O.A., Finkel, R.C., 1999. Dating fluvial terraces with ^{10}Be and ^{26}Al profiles: application to the Wind River, Wyoming. Geomorphology 27, 41–60.

Haug, G.H., Hughen, K.A., Sigman, D.M., Peterson, L.C., Rohl, U., 2001. Southward migration of the Intertropical Convergence Zone through the Holocene. Science 293, 1304–1308.

Heinrich, H., 1988. Origin and consequences of cyclic ice rafting in the Northeast Atlantic Ocean during the past 130,000 years. Quat. Res. 29, 142–152.

Hetzel, R., Niedermann, S., Tao, M.X., Kubik, P.W., Ivy-Ochs, S., Gao, B., Strecker, M.R., 2002. Low slip rates and long-term preservation of geomorphic features in Central Asia. Nature 417, 428–432.

Hughen, K.A., Overpeck, J.T., Peterson, L.C., Trumbore, S.E., 1996. Rapid climate changes in the tropical Atlantic during the last deglaciation. Nature 380, 51–54.

Hughen, K.A., Southon, J.R., Lehman, S.J., Overpeck, J.T., 2000. Synchronous radiocarbon and climate shifts during the last deglaciation. Science 290, 1951–1954.

Hughen, K.A., Eglinton, T.I., Xu, L., Makou, M., 2004. Abrupt tropical vegetation response to rapid climate changes. Science 304, 1955–1959.

Kalm, V., Mahaney, W.C., 2011. Late Quaternary glaciation in the Venezuelan (Mérida) Andes developments in Quart. Science 15, 835–841.

Kellogg, J., Bonini, W., 1982. Subduction of the Caribbean Plate and basement uplifts in the overriding South-American Plate. Tectonics 1 (3), 251–276.

Kohn, B., Shagam, R., Banks, P., Burkley, L., 1984. Mesozoic–Pleistocene fission track ages on rocks of the Venezuelan Andes and their tectonic implications. Geol. Soc. America. Memoir. 162, 365–384.

Korschinek, G., Bergmaier, A., Faesterman, T., Gerstmann, U.C., Knie, K., Rugel, G., Wallner, A., Dillmann, I., Dollinger, G., Lierse von Gostomski, C., Kossert, K., Maiti, M., Poutivsev, M., Remmert, A., 2010. A new value for the half-life of ^{10}Be by heavy-Ion elastic recoil detection and liquid scintillation counting. Nucl. Instrum. Methods Phys. Res. B 268 (2), 187–191.

Lal, D., 1991. Cosmic ray labeling of erosion surfaces: *in situ* nuclide production rates and erosion models. Earth Planet. Sci. Lett. 104, 424–439.

Lea, D.W., Pak, D.K., Peterson, L.C., Hughen, K.A., 2003. Synchroneity of tropical and high-latitude Atlantic temperatures over the last glacial termination. Science 301, 1361–1364.
Lewin, J.A., Gibbard, P.L., 2010. Quaternary river terraces in England: forms, sediments and processes. Geomorphology 120, 293–311.
Liddle, R.A., 1928. The Geology of Venezuela and Trinidad. MacGowan, Fort Worth, p. 552.
Mackenzie, A.N., 1937. Sección geológica de la región de Barinas: Distritos Barinas, Bolívar y Obispos del Estado Barinas, Venezuela. Bol. Geol. Y Min., Caracas 1 (2–4), 269–293.
Maddy, D., Bridgland, D., Westaway, R., 2001. Uplift-driven valley incision and climate-controlled river terrace development in the Thames Valley, UK. Quat. Int. 79, 23–36.
Mahaney, W.C., Kalm, V., 1996. In: Field Guide for the International Conference on Quaternary Glaciation and Paleoclimate in the Andes Mountains, June 21–July 1, 1996. Quaternary Surveys Ltd, Toronto, Canada, p. 79.
Mahaney, W.C., Milner, M.W., Voros, J., Kalm, V., Hütt, G., Bezada, M., Hancock, R.G.V., Aufreiter, S., 2000. Stratotype of the Mérida glaciation at Pueblo Llano in the Northern Venezuelan Andes. J. South Am. Earth Sci. 13, 761–774.
Mahaney, W.C., Russell, S.E., Milner, M.W., Kalm, V., Bezada, M., Hancock, R.G.V., Beukens, R.P., 2001. Paleopedology of middle Wisconsin/Weichselian Paleosols in the Mérida Andes. Venezuela. Geoderma 104, 215–237.
Masarik, J., Frank, M., Schäfer, J.M., Wieler, R., 2001. Correction of in situ cosmogenic nuclide production rates for geomagnetic field intensity variations during the past 800000 years. Geochim. Cosmochim. Acta 65 (3–4), 515–521.
Merchel, S., Herpers, U., 1999. An update on radiochemical separation techniques for the determination of long lived radionuclides via Accelerator Mass Spectrometry. Radiochim. Acta 84, 215–219.
Monod, B., Dhont, D., Hervouët, Y., 2010. Orogenic float of the Venezuelan Andes. Tectonophysics 490, 123–135.
Muscheler, R., Kromer, B., Björck, S., Svensson, A., Frieddich, M., Kaiser, K.F., Southon, J., 2008. Tree rings and ice cores reveal ^{14}C calibration uncertainties during the Younger Dryas. Nat. Geosci. 1, 263–267.
Olivero, M.L., Aguirre, J., Moncada, A., 2005a. Phenomena related to the movement of mud and debris occurred in the Páramo zone of Mérida in June 2003. Revista Forestal Venezolana 49 (2), 131–141.
Olivero, M.L., Aguirre, J., Moncada, A., 2005b. Technical information about the movement of mud and debris occurred in the Páramo zone of Mérida in june 2003. Revista Forestal Venezolana 49 (2), 143–151.
Pazzaglia, F.J., 2013. Fluvial terraces. In: Shroder, J.F. (Ed.), Treatise on Geomorphology, vol. 9. Academic Press, San Diego, pp. 379–412.
Pérez, O.J., Bilham, R., Sequera, M., Molina, L., Gavotti, P., Codallo, H., Moncayo, C., Rodriguez, C., Velandia, R., Guzmán, M., Molnar, P., 2011. GPS derived velocity field in Western Venezuela: dextral shear component associated to the Boconó fault and convergent component normal to the Andes. Interciencia 36, 39–44.
Peterson, L.C., Haug, G.H., Hughen, K.A., Rohl, U., 2000a. Rapid changes in the hydrologic cycle of the tropical Atlantic during the last glacial. Science 290, 1947–1951.
Peterson, L.C., Haug, G.H., Murray, R.W., Yarincik, K.M., King, J.W., Bralower, T.J., Kameo, K., Rutherford, S.D., Pearce, R.B., 2000b. Late Quaternary stratigraphy and sedimentation at ODP Site 1002, Cariaco basin (Venezuela). Proc. Ocean Drilling Project: Scientific Results 165, 85–99.
Peterson, L.C., Haug, H.G., 2006. Variability in the mean latitude of the Atlantic Intertropical Convergence Zone as recorded by riverine input of sediments to the Cariaco basin (Venezuela). Palaeogeogr. Palaeoclimatol. Palaeoecol. 234, 97–113.
Pierce, G.R., 1960. Geología de la cuenca de Barinas: Boleltín de Geología. In: Publicación Especial N° 3, 1, pp. 214–276.
Pigati, J.S., Lifton, N.A., 2004. Geomagnetic effects on time-integrated cosmogenic nuclide production with emphasis on *in situ* ^{14}C and ^{10}Be. Earth Planet. Sci. Lett. 226 (1–2), 193–205.
Repka, J.L., Anderson, R.S., Finkel, R.C., 1997. Cosmogenic dating of fluvial terraces, Fremont river, Utah. 794 Earth Planet. Sci. Lett. 152, 59–73.
Ritz, J.-F., Vassallo, R., Braucher, R., Brown, E.T., Carretier, S., Bourlès, D.L., 2006. Using in situ-produced ^{10}Be to quantify active tectonics in the Gurvan Bogd mountain range (Gobi-Altay, Mongolia). In: Siame, L., Bourlès, D.L., Brown, E.T. (Eds.), Special Paper 415 *in Situ*-produced Cosmogenic Nuclides and Quantification of Geological Processes. Geological Soc.. of America, pp. 87–110.
Rull, V., 2005. A middle Wisconsin interstadial in the Northern Andes. J. South Am. Earth Sci. 19, 173–179.
Salgado-Labouriau, M.L., 1984. Late-Quaternary palynological studies in the Venezuelan Andes. Erdwissenschaftliche Forschung 18, 279–293.
Schmidt, S., Hetzel, R., Kuhlmann, J., Mingorance, F., Ramos, V., 2011. A note of caution on the use of boulders for exposure dating of depositional surfaces. Earth Planet. Sci. Lett. 302, 60–70.
Schubert, C., 1974. Late Pleistocene Mérida glaciation, Venezuelan Andes. Boreas 3, 147–152.
Schubert, C., Valastro, S., 1980. Quaternary Esnujaque formation, Venezuelan Andes: preliminary alluvial chronology in a tropical mountain range. Z. der Deutschen Geologischen Gesellschaft 131, 927–947.
Schubert, C., Clapperton, C.M., 1990. Quaternary glaciations in the Northern Andes (Venezuela, Colombia and Ecuador). Quat. Sci. Rev. 9, 123–135.
Schubert, C., Vivas, L., 1993. El Cuaternario de la Coordillera de Mérida – Andes Venezolanos. Universidad de Los Andes-Fundacion Polar, Mérida, Venezuela, p. 345.
Shackleton, N.J., 1987. Oxygen isotopes, ice volume and sea level. Quat. Sci. Rev. 6, 183–190.
Shagam, R., 1972. Andean research project, Venezuela: principal dat and tectonic implications. Geol. Soc. America. Memoir. 132, 449–463.
Shagam, R., Kohn, B., Banks, P., Dasch, L., Vargas, R., Rodríguez, G., Pimentel, N., 1984. Tectonic implications of Cretaceous–Pliocene fission track ages from rocks of the circum-Maracaibo Basin region of Western Venezuela and Eastern Colombia. Geol. Soc. America. Memoir. 162, 385–412.
Soulas, J.-P., 1985. Neotectonica del flanco occidental de los Andes de Venezuela entre 701300 y 711000W (Fallas de Bocon o, Valera, Pinango y del Piedemonte). In: Memorias del VI Congreso Geológico Venezolano, Caracas, pp. 2690–2711.
Stone, J.O., 2000. Air pressure and cosmogenic isotope production. J. Geophys. Res. 105 (B10), 753–759.
Stuiver, M., Grootes, P.M., Braziunas, T.F., 1995. The GISP2 18O climate record of the past 16,500 years and the role of the sun, ocean and volcanoes. Quat. Res. 44, 341–354.
Taboada, A., Rivera, L.A., Fuenzalida, A., Cisternas, A., Philip, H., Bijwaard, H., Olaya, J., Rivera, C., 2000. Geodynamic of the Northern Andes: subductions and intracontinental deformation (Colombia). Tectonics 19 (5), 787–813.
Tricart, J., 1966. Paléoclimats et terrasses quaternaires: C.R. Somm. seances. Societé Géologique de France, pp. 202–203 (Fasc. 5).
Tricart, J., Millies-Lacroix, A., 1962. Les terrasses quaternaires des Andes vénézueliennes. Bull. Soc. Géol. France, 7e Sér. 4, 201–219.
Tricart, J., Michel, M., 1965. Monographie et carte geomorphologique de la region de Lagunillas (Andes Vénézuéliennes). Revue de Geomorphologie Dynamique 15, 1–33.
Vassallo, R., Ritz, J.F., Carretier, S., 2011. Control of geomorphic processes on ^{10}Be concentrations in individual clasts: complexity of the exposure history in Gobi-Altay range (Mongolia). Geomorphology. http://dx.doi.org/10.1016/j.geomorph.2011.07.023.
Vivas, L., 1984. El Cuaternario. La Imprenta, Mérida, p. 266.
Wegmann, K.W., Pazzaglia, F.J., 2009. Late Quaternary fluvial terraces of the Romagna and Marche Apennines, Italy. Quat. Sci. Rev. 28, 137–165.
Wesnousky, S.G., Aranguren, R., Rengifo, M., Owen, L., Caffee, M.W., Krishna, M., Pérez, O.J., 2012. Toward quantifying geomorphic rates of crustal displacement, landscape development, and the age of glaciation in the Venezuelan Andes. Geomorphology 141-142, 99–113.
Wright, J.D., 2000. Global climate change in marine stable isotope records. In: Noller, J.S., Sowers, J.M., Lettis, W.R. (Eds.), Quaternary Geochronology: Methods and Applications, vol. 4. American Geophysical Union Reference Shelf, pp. 427–433.
Zinck, A., Stagno, P., 1966. Estudio edafologico de la zona de Santo Domingo-Pagüey, Estado Barinas: Division de Obras Hidraulicas. Ministerio de Obras Publicas, Caracas.
Zinck, A., 1980. Valles de Venezuela. Cuadernos Lagoven, p. 150.